Finite quantum Heisenberg spin models and their approach to the classical limit

Larry Engelhardt* and Marshall Luban
Ames Laboratory and Department of Physics and Astronomy, Iowa State University, Ames, Iowa 50011, USA

Christian Schröder
Department of Electrical Engineering and Computer Science, University of Applied Sciences Bielefeld, D-33602 Bielefeld, Germany and Ames Laboratory, Ames, Iowa 50011, USA

(Received 24 April 2006; revised manuscript received 16 June 2006; published 11 August 2006)

We determine the temperature range over which classical Heisenberg spin models closely reproduce the zero-field susceptibility of the corresponding quantum Heisenberg models for a finite number N of interacting quantum spins s. Using mostly quantum and classical Monte Carlo methods, as well as analytical methods where applicable, we have explored a variety of geometries, including polygons, open chains, and all Platonic and several Archimedean polytopes. These systems range in size from $N=2$ to 120, and we have considered values of s from 1/2 to 50 for both antiferromagnetic and ferromagnetic exchange. Particular attention is devoted to quantifying the slow convergence of the large s quantum data to the limiting classical data. This is motivated by the desire to define conditions where classical Monte Carlo methods can provide useful predictions for finite quantum Heisenberg spin systems.

DOI: 10.1103/PhysRevB.74.054413 PACS number(s): 75.10.Jm, 75.10.Hk, 75.50.Xx, 75.40.Mg

I. INTRODUCTION

In the treatment of magnetic systems, a classical spin model is frequently used, though the microscopic moments are actually quantum in character. For example, this practice is sometimes followed in the field of magnetic molecules[1] in order to circumvent severe computational difficulties that arise in a quantum treatment. A classical model can, at times, be both conceptually illuminating and provide sufficiently accurate results. However, the accuracy of a classical model's results are generally not known, when compared to those for the quantum spins that are being represented. For that reason, the goal of the present work is to determine the circumstances under which classical models will provide a good approximation to finite systems of interacting quantum spins. In so doing, we are not only able to provide clear "rules of thumb" for specific systems; we also explore the approach to the classical limit for large values of intrinsic spin s. In order to ensure the accuracy of these comparisons, we have compared only quantum *model systems* and their classical counterparts; we have not included comparisons with experimental data, whose underlying Hamiltonian may be in question.

To this end, we have performed calculations using the Heisenberg model, describing a finite number N of interacting spins. Within this model, there are clearly a number of properties that one could calculate when trying to answer the loosely defined question, "When does a classical model accurately simulate the corresponding quantum model?" To select a suitable metric, and hence clarify this question, there are two requirements that we impose. (i) We consider a property that is of relevance to experiments, and (ii) the property, for simplicity reasons, depends on only one physically relevant parameter, such that two regimes exist—In one regime, the classical and quantum models give results that coincide to within some small prescribed error, while in the other regime they produce significantly different results. Both requirements are met by choosing to calculate the zero-field susceptibility χ as a function of temperature T and determining the minimum temperature $T_m(s)$ above which the classical and quantum results for $\chi(T)$ meet a prescribed accuracy criterion for a given choice of s. The details of this correspondence are described in Sec. II A.

In order to explore the dependence of T_m on s, we have performed calculations for a variety of systems ranging in size from $N=2$ to 120 sites, with intrinsic spin quantum numbers ranging from $s=1/2$ to, in some cases, as large as $s=50$. The classical counterpart to each quantum system is, of course, also considered, as we describe in Sec. II A. Some of these systems, specifically with $s\leqslant 5/2$, are relevant to the study of magnetic molecules.[1] Additionally, the large s calculations allow us to glean valuable information regarding the approach to the classical limit; and by studying many different sizes and geometries, we are able to judge the universality of our conclusions. While we do find certain general trends and useful rules of thumb, the diversity of the results appears to preclude a precise universal description in terms of properties of the lattices, e.g., connectivity, frustration, or symmetries.

The calculations that are necessary to explore the dependence of T_m on s pose a considerable challenge, and necessitate the use of a variety of methods. To illustrate this, for many existing magnetic molecules, matrix diagonalization of the Hamiltonian is not feasible due to the very large dimensionality of the Hilbert spaces, given by $D=(2s+1)^N$. For example, $\{Fe_{12}\}$ ($s=5/2$ and $N=12$) (Ref. 2) has $D\approx 2.2\times 10^9$, which is already pushing the current limitations of Lanczos diagonalization, while $\{Mo_{72}Fe_{30}\}$ ($s=5/2$ and $N=30$) (Ref. 3) has an associated $D\approx 2.2\times 10^{23}$. Instead we use classical and quantum Monte Carlo methods that allow us to circumvent the obstacles that large Hilbert spaces and complex multidimensional integrals pose to quantum and classical calculations, respectively. We review these methods in Sec. II C. This is preceded in Sec. II B with a discussion of the few special cases where the spectra of energy eigen-

values can be derived analytically, and matrix diagonalization is unnecessary.

In Sec. III, we present our results for a wide variety of geometries including spin chains, polygons, and a number of Platonic and Archimedean polytopes, where, for each polytope, each vertex represents a spin site and each edge connects a pair of interacting spins. We consider both antiferromagnetic (AFM) and ferromagnetic (FM) interactions, finding that for AFM interactions a classical approximation is typically valid down to a substantially lower temperature T_m than for the corresponding FM case. Furthermore, we present numerical values of T_m and explore its functional dependence on s; and to demonstrate the usefulness of these results, we compare quantum and classical calculations of $\chi(T)$ for the $\{Fe_{12}\}$ magnetic molecule[2] in Sec. III C. Finally, in Sec. IV we summarize our findings.

II. MODELS AND METHODS

A. Quantum and classical spin models

In order to compare the results of classical and quantum spin models, we use as our starting point the quantum Heisenberg model. We assume all spins to share a common quantum number s, and further assume that if a distinct pair of spins (represented $\langle i,j\rangle$) interact with one another, they do so with the same strength J_s as any other pair of interacting spins. This Hamiltonian is then given by (Ref. 4)

$$\mathcal{H} = J_s \sum_{\langle i,j\rangle} \vec{s}_i \cdot \vec{s}_j + g\mu_B \vec{H} \cdot \sum_{i=1}^{N} \vec{s}_i, \tag{1}$$

where the spin operators $\vec{s}_i$ are given in units of $\hbar$, g is the spectroscopic splitting factor, μ_B is the Bohr magneton, and $\vec{H}$ is an external magnetic field. Following Fisher,[5] the classical analog to this quantum Hamiltonian is constructed by first defining rescaled spin operators $\vec{e}_i(s) \equiv \vec{s}_i / \sqrt{s(s+1)}$, in the nature of unit vector operators, whose components satisfy the commutation relation

$$e_i^x(s)e_i^y(s) - e_i^y(s)e_i^x(s) = ie_i^z(s)/\sqrt{s(s+1)}$$

and the cyclic permutations thereof. With this replacement, and introducing the parameters, $J_c \equiv J_s s(s+1)$ and $\mu_c \equiv g\mu_B\sqrt{s(s+1)}$, Eq. (1) is rewritten

$$\mathcal{H} = J_c \sum_{\langle i,j\rangle} \vec{e}_i(s) \cdot \vec{e}_j(s) + \mu_c \vec{H} \cdot \sum_{i=1}^{N} \vec{e}_i(s), \tag{2}$$

allowing us to consider a *sequence* of Hamiltonians (2) for each geometry, where the members of a sequence differ *only* in s, sharing a common value of J_c. Since the commutators between the $\vec{e}_i(s)$ vanish in the limit of very large s, each of these sequences converge with increasing s toward a classical Hamiltonian, (Ref. 6),

$$\mathcal{H} = J_c \sum_{\langle i,j\rangle} \vec{e}_i \cdot \vec{e}_j + \mu_c \vec{H} \cdot \sum_{i=1}^{N} \vec{e}_i, \tag{3}$$

where all $\vec{e}_i$ operators are replaced by *classical* unit vectors $\vec{e}_i$.

We focus in this article on the comparison between results, derived from Eqs. (2) and (3), for the zero-field susceptibility, $\chi(T) \equiv \lim_{H\to 0} \frac{\partial M}{\partial H}$, where M is the magnetization induced by the magnetic field H. At sufficiently high temperatures, Eqs. (2) and (3) give the same values of $\chi(T)$, while at low temperatures the values of $\chi(T)$ diverge from one another. Specifically, $\chi(0)=0$ for quantum systems having a ground state with total spin $S=0$, and $\chi(T) \propto \exp(-\Delta/k_B T)$ for sufficiently small T, where Δ is the energy gap between the ground state and the first excited state for which $S>0$. Classical models, by contrast, do not have a corresponding gap in their energy spectra. As a result, an infinitesimal external magnetic field would induce a proportional (infinitesimal) magnetization, so Eq. (3) gives values of $\chi(T)$ that are nonzero in the limit $T\to 0$. For a system whose ground state has $S>0$, $\chi(T\to 0)$ diverges proportional to $1/T$, as we describe in Sec. III B.

With this high temperature correspondence (and deviation of classical and quantum results at low temperatures) in mind, we are now prepared to explicitly state the question to be answered in this article: "What is the minimum temperature $T_m(s)$ for which Eqs. (2) and (3) produce the same zero-field susceptibility $\chi(T)$ to within some predetermined factor, e.g., 2%?" This question is answered in detail in Sec. III using the methods of Secs. II B and II C, where in all cases $\chi(T)$ is obtained using the fluctuation formula $\chi(T) = (g^2\mu_B^2/3k_BT)\langle S^2\rangle_T$, where $\langle S^2\rangle_T$ denotes the ensemble average of S^2.

B. Analytical methods

For a few special geometries, it is possible to calculate the zero-field energy eigenvalues E analytically by expressing them in terms of the total spin quantum number S and additional spin quantum numbers described below. Given these energies, if one is able to calculate the degeneracy ν_E for each E, it is then straightforward to calculate the zero-field susceptibility. These special geometries can be grouped into two categories. The first category includes systems in which all spins interact equally with all other spins (sometimes referred to as "pantahedra"). In this case, the energies are given by

$$E(S,s) = \frac{J_s}{2}[S(S+1) - Ns(s+1)]. \tag{4}$$

It is also possible to write down the energies in the more general case that the spin lattice can be decomposed into two or more sublattices, such that each spin of a given sublattice (whose total spin is labeled S_A, S_B, etc.) interacts with the same strength with *all* spins of the other sublattices, but *no* spins of its own sublattice. To illustrate this, we consider two special cases, whose resulting energy spectra are very similar to Eq. (4). For a ring of four spins with nearest-neighbor interactions only, there are two sublattices, each of which consists of a pair of spins that do not interact with one another. In terms of these two sublattices, the energy spectrum is given by

$$E(S,S_A,S_B) = \frac{J_s}{2}[S(S+1) - S_A(S_A+1) - S_B(S_B+1)], \quad (5)$$

while for the octahedron there are three sublattices, resulting in

$$E(S,S_A,S_B,S_C) = \frac{J_s}{2}S(S+1) - \frac{J_s}{2}[S_A(S_A+1) + S_B(S_B+1) + S_C(S_C+1)]. \quad (6)$$

The calculation of $\chi(T)$ for these systems then reduces to enumerating all of the ways in which the individual spins of each sublattice can couple together to yield a given energy, hence providing the values of ν_E. Using these data, we are able to calculate $\chi(T)$ for very large values of s and D, which are well beyond the current limitations of matrix diagonalization. To compare with classical data, we use the results of Ref. 7, as well as additional results that have been derived for the classical $N=5$ pantahedron.[8]

C. Monte Carlo methods

For both the quantum and the classical model Hamiltonians that were shown in Sec. II A, the analytic calculation of $\chi(T)$ is not feasible for general geometries of spins. In both cases, this calculation involves an ensemble average which becomes very challenging with increasing N. For quantum spins, the value of the Hilbert space dimensionality D can become so large ($\gtrsim 10^7$) that it is impractical to attempt to compute all of the energy eigenvalues, while the classical versions often involve intractable $3N$-dimensional integrals.

Both classical and quantum Monte Carlo methods exploit the following idea. Instead of seeing it as a hindrance that one cannot include the contributions from all of the quantum eigenstates and all of the classical phase space, one can instead recognize that it is often *unnecessary* to include all of the states and use this to our advantage. When the excitation energy of a state is large relative to the thermal energy k_BT, the state will not contribute significantly to the ensemble average, and can hence be ignored. In this spirit, one can use the method of importance sampling to perform the necessary averaging, whereby the states that make large contributions are accurately sampled, and the states that make negligible contributions are ignored. (See, for example, Ref. 9.) While there are statistical errors involved in this approach, the errors can be made arbitrarily small by performing longer sampling runs. Very importantly, no systematic errors are introduced, and the statistical errors are accurately estimated during the course of a calculation.

For the quantum calculations, we use the method that was introduced in Ref. 10 and has been recently used to study similar finite systems.[11,12] The idea of this method is that a high-temperature expansion can be used to express the partition function in terms of two-spin matrix elements, which are easily evaluated.[13] The trade-off is that, in order to consider the full range of temperatures, many complicated terms must be sampled, and the Monte Carlo updating becomes very involved. However, this updating can be efficiently performed using the so-called "directed-loop" equations[10] to simultaneously satisfy detailed balance, and ergodically sample the relevant phase space. For the classical Monte Carlo calculations, importance sampling is carried out using the standard Metropolis method.[14]

Using these methods we have considered a great variety of geometries in Sec. III, with sizes ranging up to $N=120$. For this largest system, we considered quantum spins up to $s=9/2$, with dimension $D=10^{120}$. However, as impressive as this is, the quantum Monte Carlo (QMC) method also has a serious limitation. For classical systems that have frustrated ground states,[15] the quantum analogs suffer from the infamous negative sign problem,[16] and results can only be obtained for relatively high temperatures.[11] As a result, for such frustrated systems QMC calculations are *sometimes* able to provide a more complete description of experimental data than one would obtain from classical Monte Carlo. In other situations, QMC calculations are limited to temperatures that are greater than T_m, in which case QMC offers no additional information beyond that which is given by classical Monte Carlo. This issue is addressed in greater detail in the Appendix.

III. RESULTS

A. AFM interactions

In this section we present and discuss $\chi(T)$ and $T_m(s)$ data for systems of spins that interact via AFM interactions. As was described in Sec. II A, the quantity $T_m(s)$ is defined *only* in terms of some prescribed discrepancy, which we choose here to be a 2% difference between the values of χ for quantum spins s and classical spins. This value is chosen simply because a 2% difference is just visible to the eye; choosing a different number, such as 5%, does in fact lead to the same conclusions, only with a different numerical prefactor.

In Fig. 1 we show $\chi(T)$ for the square and tetrahedron with quantum spins ranging from $s=1/2$ to $s=20$ as well as classical spins. For values of $s>5/2$ we display only the results for $s=5$, 10, 15, and 20, but calculations were performed for all $s\leqslant 50$, and we observe the same trends for all values of s. Note that in both plots an arrow indicates the temperature at which a 2% difference occurs between the classical and the $s=1/2$ data, hence providing the corresponding values of $T_m\left(s=\frac{1}{2}\right)$ in terms of J_c. For both geometries we find that $k_BT_m\left(\frac{1}{2}\right)/J_c \approx 3.5$, and the values of $k_BT_m(s)/J_c$ clearly decrease toward zero with increasing s. These same trends were also found for the other structures described in Sec. II B, and thus the corresponding $\chi(T)$ data are not shown.

In Fig. 2 is shown the susceptibility per spin, $\chi(T)/N$, obtained using Monte Carlo methods, for a ring of $N=20$ spins and an Archimedean solid of $N=120$ spins, with s ranging from 1/2 to 9/2 as well as classical data. In both Figs. 1 and 2, the classical limit is indeed being approached with increasing s, but only slowly. Specifically, for $s\approx 5$ the quantum and classical results differ noticeably when $k_BT \lesssim J_c/2$; and in Fig. 1 the $s=20$ results clearly diverge from the classical curves for $k_BT \lesssim 0.01J_c$. We seek to quantify this

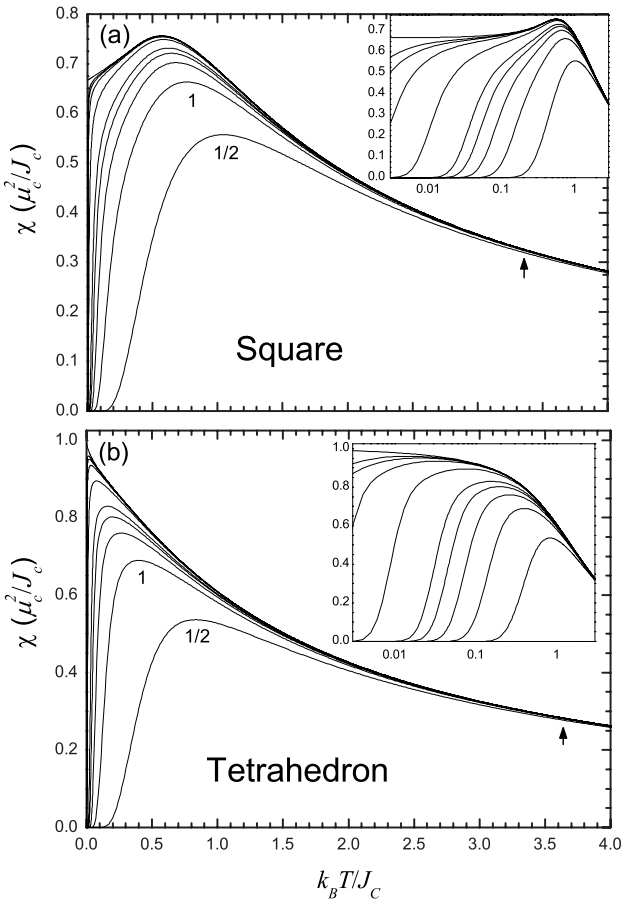

FIG. 1. Zero-field susceptibility in units of μ_c^2/J_c, where μ_c and J_c are defined in Sec. II A, for the AFM (a) square and (b) tetrahedron. In both cases, results are shown for intrinsic spins $s=1/2,1,3/2,2,5/2,5,15,20$, and classical spins. The $s=1/2$ and $s=1$ curves are labeled, and the larger values of s proceed systematically toward the classical results, which are the uppermost curves. In the inset the same data are plotted with a logarithmic temperature scale, and, as described in the text, the arrows indicate where a 2% difference is reached between the $s=1/2$ and $s=\infty$ data.

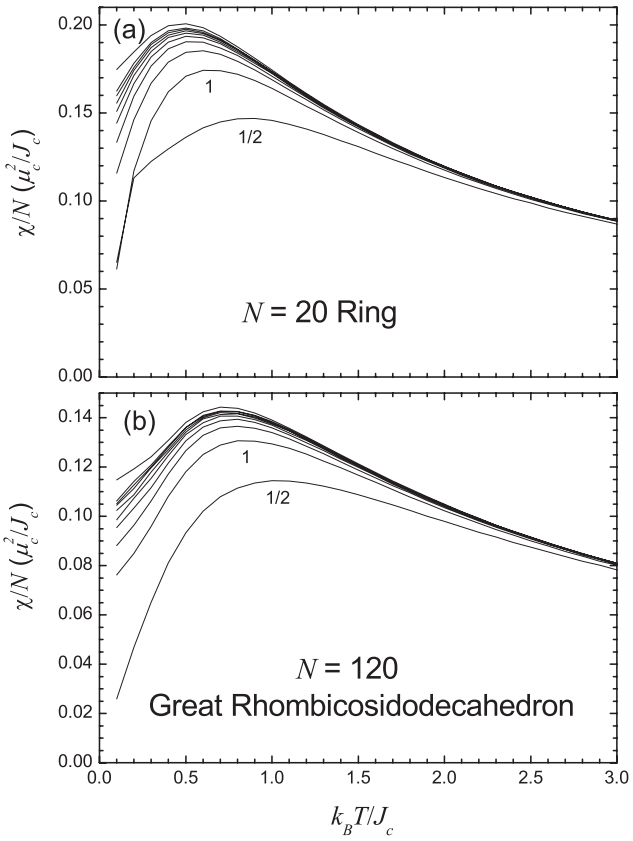

FIG. 2. Zero-field susceptibility per spin in units of μ_c^2/J_c, where μ_c and J_c are defined in Sec. II A, for the AFM (a) $N=20$ ring and (b) $N=120$ Archimedean solid (great rhombicosidodecahedron). In both cases, results are shown for intrinsic spins $s=1/2,1,\ldots,9/2$, and classical spins. The $s=1/2$ and $s=1$ curves are labeled, and the larger values of s proceed systematically toward the classical results, which are the uppermost curves.

approach to the classical limit, and have thus determined $k_BT_m(s)/J_s$, which equals $s(s+1)k_BT_m/J_c$, for many geometries.[17] One could instead analyze $k_BT_m(s)/J_c$, but, as we will show, by plotting $k_BT_m(s)/J_s$ the functional dependence of T_m on s is easily extracted.

In Fig. 3(a), we plot $k_BT_m(s)/J_s$ for the geometries described in Sec. II B, including values of s extending up to $s=20$. For all of these structures, there are clearly two distinct regimes of s values. For small s ($\lesssim 5/2$) the data increase linearly with s, and for large s ($\gtrsim 5$) the $k_BT_m(s)/J_s$ data saturate. In the intermediate range, $5/2 \lesssim s \lesssim 5$, the behavior is crossing over between the two limiting cases. [For the square, larger values of s ($\gtrsim 40$) are needed to reach saturation, but $k_BT_m(s)/J_s$ eventually approaches a constant value, ≈ 9.0.] These data immediately imply that, although $k_BT_m(s)/J_c$ decreases monotonically with s, its functional dependence is different for large and small s: For small s, $k_BT_m(s)/J_s \propto s$, or equivalently, $k_BT_m(s)/J_c \propto 1/(s+1)$; while for large s, $k_BT_m(s)/J_c \propto 1/s^2$.

In order to formulate a useful rule of thumb, we must include not only the s dependence, but also the proportionality constants. For large s there are clearly two proportionality constants that are relevant for the geometries shown in Fig. 3(a). For the dimer and square $k_BT_m/J_s \approx 9$, while $k_BT_m/J_s \approx 4.5$ for the pantahedra and octahedron. In Fig. 3(b) we have included data for $s<5$ for many additional structures, calculated using the Monte Carlo methods described in Sec. II C. Again, we find that in *all* cases, k_BT_m/J_s increases linearly with s for small s, and then approaches saturation for larger s. For the pantahedra and octahedron this saturation is already reached by $s \approx 2$, while k_BT_m/J_s continues to increase for the other structures. In fact, other than the pantahedra and octahedron, all of these data for $s \leqslant 3$ can be described to within 30% by the function $k_BT_m(s)/J_s \approx 2(s+1)$, giving the very simple rule of thumb, $k_BT_m/J_c \approx 2/s$ for this interval of s.

B. FM interactions

The same systems (described in the Appendix) but with FM interactions were also studied in the same manner as was

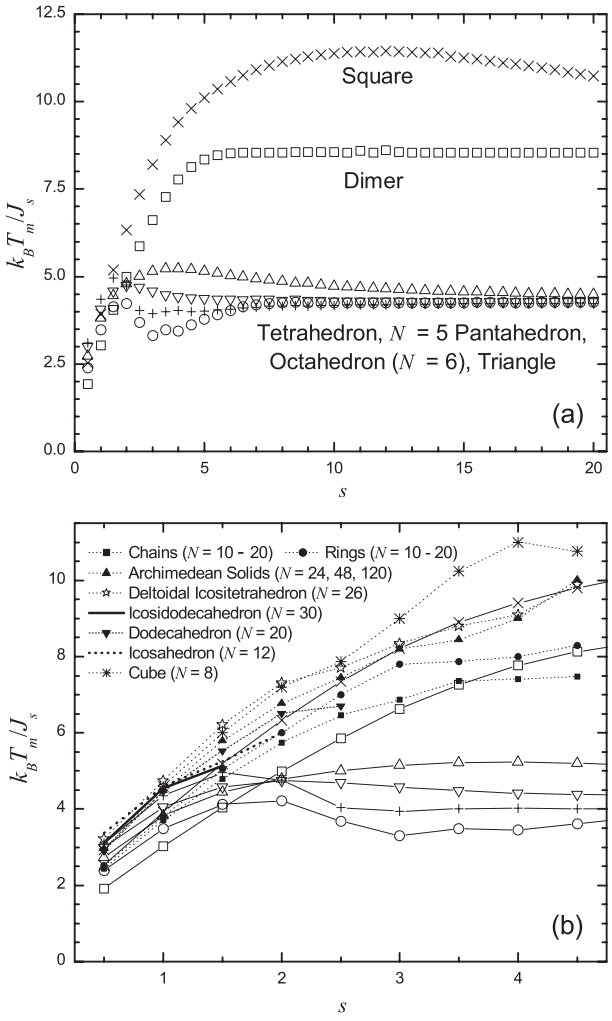

FIG. 3. T_m vs s for systems with AFM interactions. In (a) data are included up to $s=20$ for the dimer (□), triangle (○), square (x), tetrahedron (Δ), $N=5$ pantahedron (∇), and octahedron (+). The same symbols also apply in (b), where data are plotted for all of the geometries that have been considered. As a guide to the eye, lines connect successive data points. For additional details regarding these data and geometries, see the Appendix.

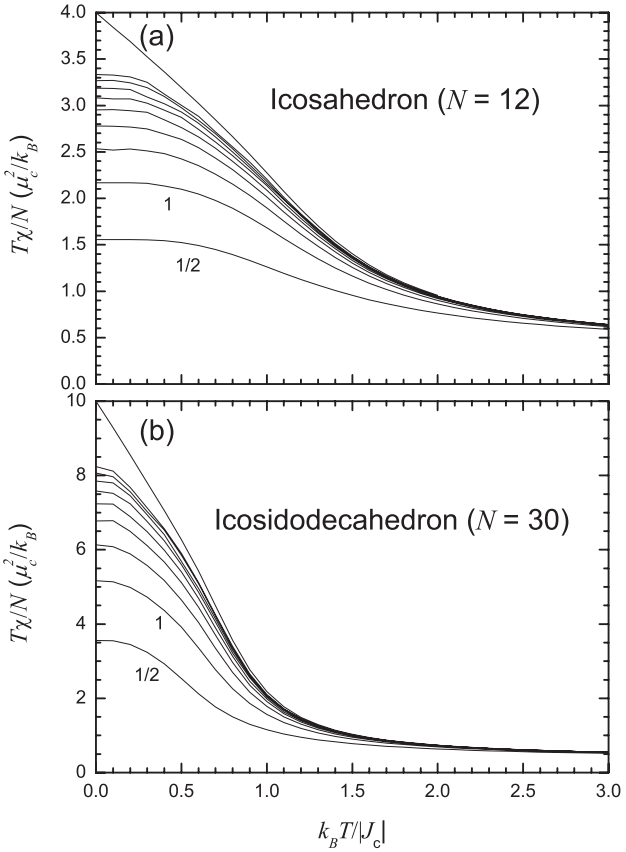

FIG. 4. The product of temperature times zero-field susceptibility per spin in units of μ_c^2/k_B for the FM (a) icosahedron and (b) icosidodecahedron. In both cases, results are shown for intrinsic spins $s=1/2,1,\ldots,9/2$, and classical spins. The $s=1/2$ and $s=1$ curves are labeled, and the larger values of s proceed systematically toward the classical result, which are the uppermost curves.

described for AFM systems. There are, however, some distinct differences between the AFM and FM results. When all interactions are FM, the ground states of the classical systems are realized by aligning all spins; similarly, the ground states of the quantum systems have $S=Ns$. As a result, $\chi(T)$ diverges at low T proportional to $1/T$ in all cases, so instead of plotting $\chi(T)$, it is more instructive to plot $T\chi(T)$ as is shown in Fig. 4. Moreover, the limiting $T\to 0$ values of $T\chi$, henceforth referred to as $(T\chi)_0$, converge with increasing s to the classical result.[18] Consequently, there will be some value of $s\equiv s^*$ which, when exceeded, will give results that differ by less than 2% even at $T=0$. Therefore, $T_m=0$ for $s>s^*$, so for large s we do not obtain the AFM result, i.e., $k_BT_m(s)/J_c \propto 1/s^2$. Note however that the value of s^* is typically quite large (e.g., $s^*=45$ for $N=10$), and there is still a large region of s values, shown in Fig. 5(a), for which k_BT_m/J_s is independent of s, or equivalently, $k_BT_m(s)/J_c \propto 1/s^2$.

As shown in Fig. 5, k_BT_m/J_s indeed decreases for large s as s^* is approached, but the data are nonetheless quite similar to those obtained for the AFM systems. For $s\lesssim 5$, k_BT_m/J_s is increasing, and this increase is again linear with s. The most striking feature of Fig. 5 is perhaps that k_BT_m/J_s can be quite large, exceeding 30 for the case of the $N=5$ pantahedron and the octahedron, and exceeding 10 for almost all of the systems when $s\gtrsim 5/2$. There is a very large variation in the data between the geometries, but the median values of T_m can be roughly described by $k_BT_m/J_s \approx 5s$ for $s\lesssim 5$. Comparing with the AFM rule of thumb, for small s these values of T_m are similar to those found for AFM interactions, but for large s, T_m is much larger when the interactions are FM.

C. An application: Fe_{12}

To illustrate the applicability of the data presented here (in Figs. 3 and 5) to the analysis of experimental results, we now compare quantum and classical calculations of the zero-field susceptibility for an existing system for which the quantum

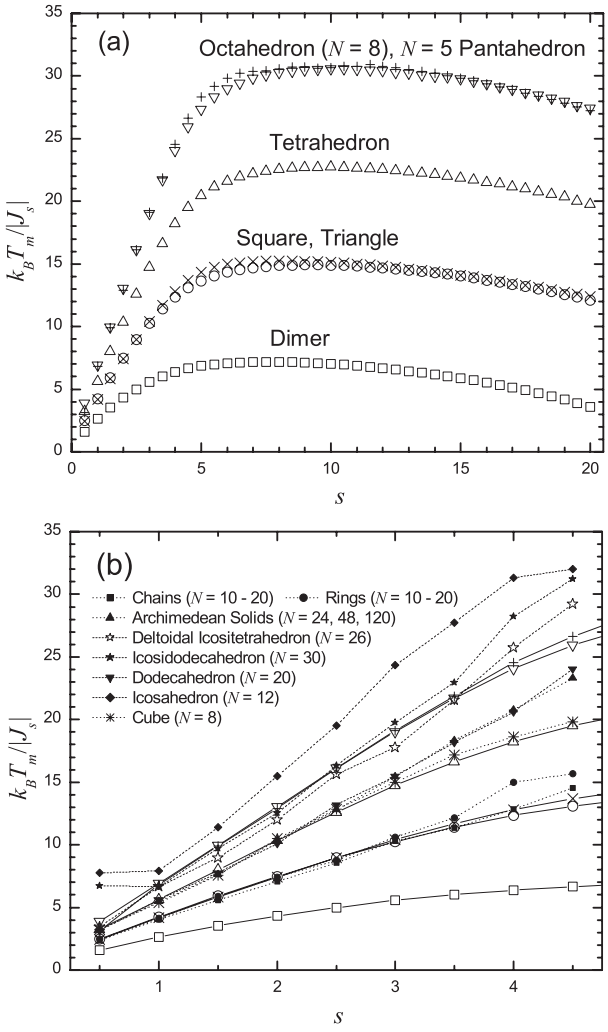

FIG. 5. T_m vs s for systems with FM interactions. In (a) data are included up to $s=20$ for the dimer (□), triangle (○), square (×), tetrahedron (△), $N=5$ pantahedron (▽), and octahedron (+). The same symbols also apply in (b), where data are plotted for all of the geometries that have been considered. As a guide to the eye, lines connect successive data points. For additional details regarding these data and geometries, see the Appendix.

calculations are challenging. The $\{Fe_{12}\}$ magnetic molecule[2] is comprised of a ring of 12 Fe^{3+} ions ($s=5/2$), such that $D=6^{12}\approx 2.2\times 10^9$, which is too large to allow the full Hamiltonian to be diagonalized using current computers. By analyzing the measured[19] high-field magnetization of $\{Fe_{12}\}$ using QMC calculations, we have recently[12] estimated the exchange constant for this system to be $J_s/k_B=35.2$ K, assuming $g=2.0$. Given this estimation, we now compare the temperature dependence (in Kelvin) of $\chi(T)$, as calculated using a model $\{Fe_{12}\}$ Hamiltonian, assuming Heisenberg interactions, for both quantum ($s=5/2$) and classical ($s\to\infty$) spins, shown in Fig. 6.

Upon inspecting Fig. 3, one finds that $T_m\approx 7J_s/k_B$ for an AFM ring, which gives a value of $T_m\approx 7\times 35.2$ K for $\{Fe_{12}\}$, which is slightly less than 250 K. In Fig. 6 we present the corresponding theoretical curves for $\chi(T)$, with the precise

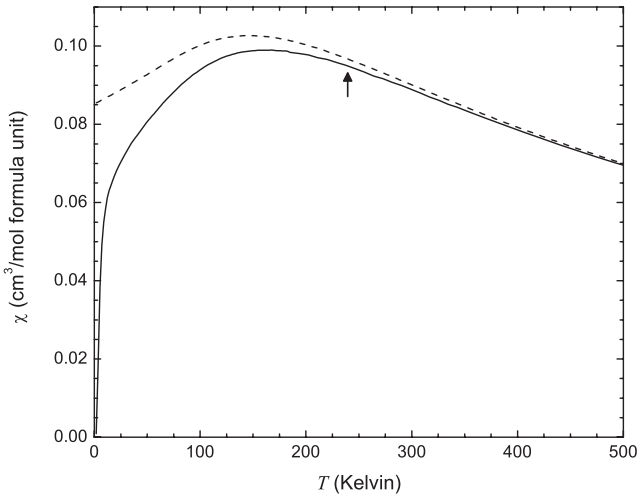

FIG. 6. Calculated molar susceptibility vs T for the $\{Fe_{12}\}$ magnetic molecule (Ref. 2). Data are included for both the quantum ($s=5/2$) Hamiltonian (solid), as calculated using QMC, and the classical Hamiltonian (dashed). Both calculations assume $J_s/k_B=35.2$ K, as estimated in Ref. 12, and $g=2.0$. The arrow indicates the temperature T_m above which these two data sets differ by less than 2%.

value of T_m indicated by an arrow. It is interesting to note that for this system the quantum and classical results differ significantly over most of the temperature range of experimental interest ($T<300$ K). Furthermore, for $T\lesssim 150$ K, the results diverge from one another, such that the use of these classical results for the analysis of experimental data would introduce significant systematic errors into one's estimation of the exchange parameters. However, for systems with smaller values of J_s, classical results can potentially be used to much lower temperatures, the values of which can be accurately estimated from Figs. 3 and 5.

IV. SUMMARY

In this article we have utilized a combination of quantum Monte Carlo, classical Monte Carlo, and analytical methods to study and quantify how, with increasing intrinsic spin s, the results of quantum Heisenberg model systems approach the results of the corresponding classical Heisenberg models. To this end, the zero-field susceptibility was calculated for many geometries, and from these data we have extracted the minimum temperature $T_m(s)$ at which the quantum (spin s) results differ by less that 2% from the corresponding classical results. In terms of the exchange constants J_s and J_c (defined in Sec. II A) we have found for small s that $k_B T_m/J_s\propto s$, or equivalently $k_B T_m/J_c\propto 1/(s+1)$, while for large s we found that $k_B T_m/J_s$ saturates, and thus $k_B T_m/J_c\propto 1/s^2$. In addition to these general trends, the precise dependence of T_m has been obtained for many specific systems and can be found by inspecting Figs. 3 and 5. We have also attempted to find a universal dependence of T_m on s in terms of various properties of the lattices (e.g., connectivity, frustration, or symmetries), which would allow one to describe

$T_m(s)$ in terms of a *single* function, applicable to all geometries. However, such universality does not appear to be present, given the diversity of the results in Figs. 3 and 5. Nevertheless, it *is* possible to formulate certain "rules of thumb" that are precise enough to be of value when attempting to formulate a rough estimation of the temperature range for which a classical model will be useful. In particular, for almost all of the AFM systems that we have studied, T_m can be described to within 30% by the rule-of-thumb $k_B T_m/J_c \approx 2/s$, which is valid for $s \lesssim 3$ and should therefore be relevant to the analysis of experimental susceptibility data. When FM interactions are present we have found that, to within a factor of two, the rule-of-thumb $k_B T_m/J_c \approx 5/(s+1)$ applies for $s \lesssim 5$.

The application of these results to the analysis of a real system of interacting quantum spins would be straightforward, provided one had some estimate of the relevant energy scale J_s. For example, inspection of Fig. 3(b) shows that a classical model will accurately reproduce the results of quantum spins $s=3/2$ for temperatures $T \gtrsim (5 \pm 1) J_s/k_B$. A more specific example has also been provided in Sec. III C, wherein we show that a classical Hamiltonian will accurately describe the $\{Fe_{12}\}$ magnetic molecule only for $T \gtrsim 250$ K. Additionally, the present large s results [shown in Fig. 3(a)] also underscore the fact that a huge value of s does *not* automatically imply that a classical spin model is valid. For example, a spin triangle with an exchange constant $J_s/k_B = 10$ K could accurately be described by a classical model only for $T \gtrsim 40$ K, even if $s=50$. Finally, we remark that these results are only meant to provide information about *static* properties. Obtaining classical and quantum time-correlation functions and comparing them in an analogous manner should provide interesting and useful results and would be a worthy avenue for future study.

ACKNOWLEDGMENTS

Ames Laboratory is operated for the United States Department of Energy by Iowa State University under Contract No. W-7405-Eng-82.

APPENDIX: DESCRIPTION OF GEOMETRIES

The various geometries studied here can almost all be placed into one of three general categories: Open chains, closed rings (polygons), or three-dimensional polytopes. For the chains and rings, we find that with increasing N the results for $T_m(s)$ rapidly converge to a single curve that is essentially independent of N and is valid for both even and odd N. The data labeled "chains" and "rings" in Figs. 3(b) and 5(b) are hence averages over these data with N varying from 10 to 20. (For the classical open chains, the exact susceptibility has long been known,[5] and these exact results are used here.) The category of chains also includes the simplest possible case, which is one pair of interacting spins (dimer), while the rings include the triangle and square. Data for these three systems each appear separately in Figs. 3 and 5.

The polytopes that were studied include four of the 13 Archimedean solids (AS) and all five Platonic solids (PS). (A complete description of all of these polytopes can be found in Ref. 20.) Of these AS, three of the structures were chosen because they are the only nonfrustrated AS that exist (i.e., they are bipartite lattices), and hence allow QMC calculations to proceed down to arbitrarily low T, even for AFM exchange. They are the truncated octahedron ($N=24$), great rhombicuboctahedron ($N=48$), and great rhombicosidodecahedron ($N=120$). They also share an additional property: As is the case with large N chains and rings, these three AS produce the same values of $T_m(s)$, independent of N, so their averages also appear in Figs. 3(b) and 5(b), labeled "Archimedean solids."

Recall from Sec. III B that s^* depends on N, which implies for $s \leq s^*$ that T_m must also depend on N. For $s<5$ however, we find that the variation of T_m with N is always smaller than the associated error bars for the chains, rings, and nonfrustrated AS. For small s, these error bars are smaller than the symbols that appear in Figs. 3(b) and 5(b), while for $s=9/2$ the uncertainties in $k_B T_m/J_s$ are roughly ± 1. In Figs. 3(a) and 5(a), the errors are considerably smaller than the associated symbols for all s.

The remaining AS that we studied is the icosidodecahedron, whose structure is adopted by multiple species of magnetic molecules.[3,11,21,22] For this geometry, AFM interactions give rise to a classical ground state configuration that is frustrated,[23] so the QMC calculations are restricted to relatively high T.[16] Specifically, these QMC calculations for $T < T_m$ were possible only with $s=1/2$, 1, and 3/2. Frustration also occurs for four of the five PS, the cube being the one exception. Two of the PS, the tetrahedron and octahedron, although being frustrated, were calculated using the method of Sec. II B; while for the other two PS, the icosahedron and dodecahedron, QMC calculations were used. For the icosahedron, we were able to proceed to temperatures below T_m for $s \leq 2$, and, for the dodecahedron, could handle all $s \leq 5/2$. Consequently, data for larger s do not appear in 3(b) for the icosidodecahedron, icosahedron, and dodecahedron.

There are two other geometries for which $\chi(T)$ and T_m have also been calculated: The $N=5$ pantahedron and the deltoidal icositetrahedron.[20] The pantahedra were described in Sec. II B, and the deltoidal icositetrahedron is a polytope which is unfrustrated and of lower symmetry than the PS or AS. For both of these structures, the resulting $k_B T_m/J_s$ data appear in Figs. 3(b) and 5(b). In order to obtain the T_m data that have been presented here, a great deal of additional $\chi(T)$ data were obviously calculated which have not been shown; these data are available from the authors for all of the structures.

*Electronic address: lengelhardt@fmarion.edu

[1] A recent useful survey of magnetic molecules is given in R. E. P. Winpenny, Comp. Coord. Chem. II **7**, 125 (2004).
[2] A. Caneschi, A. Cornia, A. Fabretti, and D. Gatteschi, Angew. Chem., Int. Ed. **38**, 1295 (1999).
[3] A. Müller, M. Luban, C. Schröder, R. Modler, P. Kögerler, M. Axenovich, J. Schnack, P. Canfield, S. Bud'ko, and N. Harrison, ChemPhysChem **2**, 517 (2001).
[4] Tildes, written below symbols, are used to distinguish quantum operators from their classical counterparts.
[5] M. E. Fisher, Am. J. Phys. **32**, 343 (1964).
[6] Operators and c numbers are of course distinct mathematical objects. However, in the limit $s \to \infty$, Eq. (2) is equivalent to Eq. (3) in the sense that they both yield the same energy spectra and thermodynamic data.
[7] O. Ciftja, M. Luban, M. Auslender, and J. H. Luscombe, Phys. Rev. B **60**, 10122 (1999).
[8] M. Luban (unpublished).
[9] D. P. Landau and K. Binder, *A Guide to Monte Carlo Simulations in Statistical Physics* (Cambridge University Press, Cambridge, 2000).
[10] O. F. Syljuåsen and A. W. Sandvik, Phys. Rev. E **66**, 046701 (2002).
[11] A. Müller, A. Todea, J. van Slageren, M. Dressel, H. Bögge, M. Schmidtmann, M. Luban, L. Engelhardt, and M. Rusu, Angew. Chem., Int. Ed. **44**, 3857 (2005).
[12] L. Engelhardt and M. Luban, Phys. Rev. B **73**, 054430 (2006).
[13] D. C. Handscomb, Proc. Cambridge Philos. Soc. **60**, 115 (1964).
[14] N. Metropolis, A. W. Rosenbluth, M. N. Rosenbluth, A. M. Teller, and E. Teller, J. Chem. Phys. **21**, 1087 (1953).
[15] R. Moessner and A. P. Ramirez, Phys. Today **59**(2), 24 (2006).
[16] M. Troyer and U.-J. Wiese, Phys. Rev. Lett. **94**, 170201 (2005).
[17] Descriptions of the geometries, as well as some technical details regarding the results for different geometries, are contained in the Appendix.
[18] For FM exchange, the ground state has $S=Ns$, and the values of $(T\chi)_0$ are easily calculated from the fluctuation formula for the cases of both classical and quantum spins. For quantum spins, $(T\chi)_0=\frac{\mu_e^2}{3k_B}\frac{N(Ns+1)}{s+1}$; and for classical spins, $(T\chi)_0=\frac{\mu_e^2}{3k_B}N^2$.
[19] Y. Inagaki, T. Asano, Y. Ajiro, Y. Narumi, K. Kindo, A. Cornia, and D. Gatteschi, J. Phys. Soc. Jpn. **75**, 1178 (2003).
[20] URL http://mathworld.wolfram.com
[21] B. Botar, P. Kögerler, and C. L. Hill, Chem. Commun. (Cambridge) **25**, 3138 (2005).
[22] B. Botar, P. Kögerler, and C. L. Hill, J. Am. Chem. Soc. **128**, 5336 (2006).
[23] M. Axenovich and M. Luban, Phys. Rev. B **63**, 100407(R) (2001).